Modulated order in classical magnetoelastic chains

Mario Marchand* and Alain Caillé
Département de Physique et Centre de Recherche en Physique du Solide, Université de Sherbrooke, Sherbrooke, Québec, Canada J1K 2R1

(Received 4 December 1987; revised manuscript received 10 May 1988)

We investigate the nature of modulated lattice distortions that can occur in a two-dimensional array of classical magnetoelastic chains coupled together by elastic interactions only. The phase diagram for the lattice structure is obtained by numerically minimizing a one-dimensional, temperature-dependent, effective-free-energy functional of the elastic variables. At zero temperature, only phases where the winding number is uniquely defined are found, and the transitions among these phases are suggestive of a complete devil's-staircase behavior. These numerical results are consistent with N. Ishimura's analytic demonstration that such a staircase exists [J. Phys. Soc. Jpn. **54**, 4752 (1985)]. At finite temperatures, phases where the winding number is not uniquely defined are found and, in addition, first- and second-order transitions appear. Also of interest are superdegenerate lines where the equilibrium phase is composed of noninteracting solitons of zero energy.

I. INTRODUCTION

Spin-lattice models, in which a local order parameter couples to the elastic deformations, are useful for describing structural phase transitions.[1,2] These approaches, where the elastic variables are treated in the continuum approximation, although successful for handling long-wavelength instabilities, are not suited to deal with short-wavelength situations. Recently,[3,4] however, it was shown that periodically modulated structures of short wavelengths can occur in discrete spin-lattice models. Indeed, the magnetoelastic model of De Simone, Stratt, and Tobochnik[3] is known to be equivalent to the axial next-nearest-neighbor Ising (ANNNI) model[5-8] and, as shown by Ishimura,[4] the ground-state phase diagram of an Ising magnetoelastic chain exhibits a devil's staircase.[9,10] In this paper we study a simple magnetoelastic model containing both first-neighbor elastic interactions and finite-temperature effects. As such, it is a generalization of the models of Refs. 3 and 4. We shall see that these generalizations will bring about interesting new results.

The model consists of one-dimensional (1D) classical spin chains interacting with three-dimensional (3D) elastic variables. It is already known[11-13] that even if the 1D interacting spin system cannot sustain long-range magnetic order at a finite temperature T, it can create, by means of a magnetoelastic coupling, nonuniform lattice instabilities and thus a phase transition at finite T for the elastic variables interacting in three dimensions. Since the spin-exchange interaction depends on the bond length, the lattice distortion affects the short-range magnetic order and thus its long-range order at $T=0$ in the distorted lattice phase. In this way, the magnetoelastic coupling changes the form of the long-range and the short-range order present in the bare lattice and the bare 1D magnetic system.

For homogeneous translationally invariant models, it has been shown[12,13] that the equilibrium lattice structure is always uniform when only first-neighbor interactions are present, that dimerization can be triggered by second-neighbor elastic interactions, and finally that modulated structures of a period longer than two can occur when third-neighbor elastic interactions are included. In this paper we consider models without translational invariance. As is usual in microscopic models[2,14,15] of structural phase transitions, the substrate potential seen by each particle is intended to mimic the effect of a rigid background offered by the other atoms. As is shown in Refs. 3 and 4, one then finds that only first-neighbor interactions are needed to obtain periodically modulated phases. In order to investigate the kind of modulated order that can result from a magnetoelastic coupling alone, we present a model where the equilibrium lattice structure is always uniform (unmodulated) in the absence of a magnetoelastic coupling. Therefore, frustration results, in our case, only from the magnetoelastic coupling.

As in Ref. 12, the equilibrium lattice structure is obtained from the configuration of lowest energy (the ground state) of an exact free-energy functional of the elastic variables obtained by integrating over the spin variables. From this free-energy functional, it is easily seen that effective nonconvex[14,15] first-neighbor interactions arise as a result of the magnetoelastic coupling. We use the powerful numerical algorithm proposed recently by Griffiths and Chou[16,17] to find the ground state of this free-energy functional. This algorithm has the advantage of not postulating, *a priori*, the form of the ground-state configuration. It is based on a minimization eigenvalue equation which focuses directly on the ground state instead of searching for it among all the extrema of the free energy as is usually done.[6-8] This last property is very useful since the two-dimensional (2D) map that results from the extremum condition[14,15] (when the range of the

interactions is limited to first neighbors) is, in general, multivalued in the presence of nonconvex interactions.

The phase diagram obtained is very complex. At $T=0$, our model reduces to that of Ishimura[4] and our numerical results are suggestive of a devil's-staircase behavior in accordance with Ishimura's results. At finite temperature, the free-energy functional resembles that of model 2 of Refs. 14 and 15 and similar results are obtained: a devil's-staircase behavior for transitions among "convex" phases[14,15] (where all the particles experience only the convex part of the interacting potential) and first- and second-order transitions among "nonconvex" phases[14,15] (where some of the particles experience the nonconvex part of the interacting potential). Also of interest are lines in parameter space where the ground state of the free energy is infinitely degenerate. Along these *superdegenerate* lines,[18] the lattice structure is seen to be formed of noninteracting solitons of zero energy. At finite temperature, phases where the winding number is not uniquely defined (i.e., two numbers instead of one are needed to identify the phase) are found whereas only phases where the winding number is uniquely defined are found at $T=0$. We have also identified a point in parameter space where a superdegenerate point breaks into triple points. The phase diagram around this point is seen to be similar to the one found recently by Yokoi, Tang, and Chou[19] for the chiral XY model.

The organization of this paper is as follows. The model is presented in Sec. II and the free-energy functional for the elastic variables is derived in Sec. III. The numerical results, including the phase diagram for the lattice structure, superdegenerate points, and tricritical points, are presented in Sec. IV. Finally, our results are summarized and discussed in Sec. V.

II. THE MODEL

To study the nature of the lattice distortions that may occur in a 2D array of classical spin chains coupled together by elastic interactions, it is important to avoid unnecessary complications. Thus we assume that all the elastic interchain couplings are identical and sufficiently strong so as to achieve a 3D structural long-range order with all the elastic variables in phase with their interchain nearest neighbors. In this case, the identical distortion (if any) of each chain can only be modulated along one direction and all the transverse couplings need not be included in the Hamiltonian when using a mean-field approach. This kind of elastic anisotropy can be found in certain quasi-one-dimensional magnetic systems[20,21] that have a high-temperature structural rearrangement which prepares the softening of the lattice in one particular direction without softening in the other two directions. Therefore, for such physical problems, we propose the following 1D Hamiltonian:

$$H=H_e+\sum_{i=1}^{\infty} J(u_{i+1}-u_i)\mathbf{S}_i\cdot\mathbf{S}_{i+1} , \tag{2.1}$$

with the elastic part H_e of the Hamiltonian given by

$$H_e=\sum_{n=1}^{\infty}[\tfrac{1}{2}K_0u_n^2+K_1(u_{n+1}-u_n)^2] , \tag{2.2}$$

u_n is the displacement of the nth particle with respect to some reference position, here assumed to be a regular 1D lattice of equally spaced points. These particles also possess classical spin degrees of freedom which are described by an n-vector $\mathbf{S}_i$ interacting with first neighbors through the exchange integral J, which is a function of the atom's spacing. In this paper we consider the simplest case where J depends linearly on the atomic spacing:

$$J(u_{n+1}-u_n)=J_0-J_1(u_{n+1}-u_n) , \tag{2.3}$$

where J_0 and $-J_1$ are, respectively, the value of J and its gradient evaluated at $(u_{n+1}-u_n)=0$. J_1 is thus the magnetoelastic coupling. Although a modification of this linear dependence could change the behavior of the results, we limit ourselves to (2.3), this expansion being always valid for small displacements.

The term $\frac{1}{2}K_0u_n^2$ in (2.2) is physically interpreted as the local potential experienced by a particle in the nth cell as a result of the interaction with the rigid background. This unbounded local potential, although useful for describing structural phase transitions,[2] is not appropriate for materials where particles can jump from one unit cell to another. Hence, this local potential confines each particle to its cell and the average lattice distortion $\langle u_{n+1}-u_n\rangle$ must be zero for an equilibrium lattice structure:

$$\lim_{N\to\infty}\frac{1}{N}\sum_{n=1}^{N}(u_{n+1}-u_n)=0 . \tag{2.4}$$

Were this not so then, with $\langle u_{n+1}-u_n\rangle=\delta$, the energy $E(N)$ of a chain of N atoms would increase dramatically with N:

$$E(N)\sim\sum_{n=1}^{N}K_0(n\delta)^2 . \tag{2.5}$$

Hence, adding a pressure term proportional to $(u_{n+1}-u_n)$ to (2.2) would have no effect on the equilibrium lattice structure. However, the action of a pressure could be simulated, in a first approximation, by changing J_0 and keeping K_0, K_1, J_1 constant.

$J_1=0$, the spins decouple entirely from the elastic variables, and from (2.2) it is easily seen that the equilibrium lattice structure is that of the uniform phase $\{u_n=0\}$. More generally, it has been shown[13,15] that the ground state of (2.2) is always uniform for a convex substrate potential and for convex first-neighbor interactions. *Hence, periodically modulated lattice phases can only occur in this model for a nonzero value of the magnetoelastic coupling* J_1.

III. EXACT FREE-ENERGY FUNCTIONAL OF THE ELASTIC VARIABLES

As in Ref. 12, the 3D equilibrium lattice structure is the ground state of the following temperature-dependent free-energy functional F_e of the elastic variables:

$$e^{-\beta F_e}=e^{-\beta H_e}\operatorname*{tr}_{\{S_i\}}e^{-\beta\left[\sum_{i=1}^{\infty}J(u_{i+1}-u_i)\mathbf{S}_i\cdot\mathbf{S}_{i+1}\right]} , \tag{3.1}$$

where $\beta=(k_B T)^{-1}$. This mean-field approach, although useful for finding the equilibrium structures, can only yield the classical critical exponents. In this work, we will be only concerned with the equilibrium phases.

For the Ising model ($n=1$), the trace in (3.1) has the following meaning:

$$\operatorname*{tr}_{\{S_i\}} = \tfrac{1}{2}\sum_{S_1}\tfrac{1}{2}\sum_{S_2}\cdots\tfrac{1}{2}\sum_{S_N}, \tag{3.2a}$$

where each sum is restricted to the two possible values of $S_i=\pm 1$. For the Heisenberg model ($n=3$), the trace in (3.1) becomes

$$\operatorname*{tr}_{\{S_i\}} = \int\frac{d\Omega_1}{4\pi}\int\frac{d\Omega_2}{4\pi}\cdots\int\frac{d\Omega_N}{4\pi}, \tag{3.2b}$$

where the $d\Omega_i$ are the spherical solid angle elements. Because of the unidimensionality of the spin interactions and the rotational invariance of the Hamiltonian, these integrations can be performed exactly.[12] We immediately find

$$F_e=H_e+\sum_{i=1}^{\infty}\Psi[J(u_{i+1}-u_i)], \tag{3.3}$$

where $\Psi(J)$ is defined by

$$\Psi(J)\equiv-\beta^{-1}\ln[\cosh(\beta J)] \quad \text{(Ising)}, \tag{3.4a}$$

$$\Psi(J)\equiv-\beta^{-1}\ln\left[\frac{\sinh(\beta J)}{\beta J}\right] \quad \text{(Heisenberg)}. \tag{3.4b}$$

At $T=0$, for all n-vector models, $\Psi(J)$ becomes

$$\Psi(J)=-|J| \quad (T=0), \tag{3.5}$$

where $|x|$ means the absolute value of x.

The form of $\Psi(J)$ leads us directly to the mechanism responsible for structural instabilities in the model given by (2.1). The ground-state energy of a pair of spins interacting with an exchange integral J is $-|J|$. Indeed for J positive or negative, the spins align themselves, respectively, antiferromagnetically or ferromagnetically at $T=0$, giving the result (3.5). Hence, for nonzero magnetoelastic coupling, the atoms displace themselves in order to minimize the total energy which includes the contribution $-|J|$ of their spin degrees of freedom and, in this manner, the lattice becomes polarized.[3] At finite temperature, this effect is reduced due to an entropy contribution resulting from a nonzero occupation probability of the excited spin states. In addition, $\Psi(J)$ shows a continuous variation near $J=0$ at finite T. This reflects the fact that the spin-state energies and the occupation probability of the states vary continuously with J. It is only the ground-state energy that varies discontinuously because of the discontinuous change of the ground state from ferromagnetic (FM) to antiferromagnetic (AF) at $J=0$. *Hence, it is the possibility of inverting the sign of the exchange integral, as a function of the interparticle distance, that permits the occurrence of lattice instabilities in Hamiltonians of the form (2.1).* This feature is to be contrasted with the quantum spin-Peierls transition[20] where it is not needed.

The polarization action of the spins is less effective for continuous Heisenberg spins than for discrete Ising spins. This is revealed in the expansion of (3.4) for $J\ll\beta^{-1}$:

$$\Psi(J)=-\tfrac{1}{2}\beta J^2 \quad \text{(Ising)}, \tag{3.6a}$$

$$\Psi(J)=-\tfrac{1}{6}\beta J^2 \quad \text{(Heisenberg)}. \tag{3.6b}$$

Apart from quantitative differences, the lattice structure phase diagrams are expected to be qualitatively the same for these two models since their function $\Psi(J)$ is similar. For this reason, the numerical calculations in Sec. III are performed for the Ising model only.

Equation (3.3) is written as

$$\tilde{F}_e=\sum_{n=1}^{\infty}[\tfrac{1}{2}x_n^2+\psi(x_{n+1}-x_n-\nu)], \tag{3.7a}$$

$$\psi(x)\equiv\kappa x^2+\Psi(J), \tag{3.7b}$$

$$x_n\equiv J_1 u_n/(J_1^2/K_0), \tag{3.7c}$$

$$\kappa\equiv K_1/K_0, \tag{3.7d}$$

where $\tilde{F}_e$ and ν are, respectively, F_e and J_0 scaled in units of J_1^2/K_0. In (3.7b), $\Psi(J)$ is (3.4a) for the Ising case and (3.4b) for the Heisenberg case where β is scaled by K_0/J_1^2. The reduced temperature τ is defined by $\tau=\beta^{-1}/(J_1^2/K_0)$. This choice of energy unit is more appropriate than $J_1^2/2K_1$ (Ref. 12) made for translationally invariant models since the ground state of (3.7) exists and is, *a priori*, nontrivial when $K_1=0$.

From (3.7) and (3.4), the magnetoelastic coupling is seen to generate an effective nonconvex first-neighbor interaction and, therefore, in solving (3.7), we seek a better understanding of both magnetoelastic systems and systems with nonconvex interactions.[14,15] In particular it is interesting to see to what extent the features present in the phase diagrams of Refs. 14 and 15 remain in the phase diagram of (3.7).

IV. NUMERICAL RESULTS

The numerical algorithm proposed recently by Griffiths and Chou[16,17] is used to find the phase diagram as a function of κ, τ, and ν. The notation and a description of the algorithm that we have used is presented in Sec. III of Ref. 15. The phases are identified by the winding number ω:

$$\omega=\frac{1}{Q}\sum_{n=1}^{Q}\Theta(x_{n-1}-x_n), \tag{4.1}$$

where Q is the period of the state (we restrict ourselves to states of finite periodicity), $x_0=x_Q$ and $\Theta(x)=+1$ (if $x\geq 0$), and $\Theta(x)=0$ (if $x<0$). Note that the numerator and denominator are two separate integers so that, in this way, we can distinguish between the state $\omega=\frac{1}{2}$, which has $Q=\frac{1}{2}$, and the state $\omega=\frac{2}{4}$, which as $Q=4$ (see Fig. 1 of Ref. 15).

A. The phase diagram for the lattice structure

As in Refs. 12–15, $\psi(x)$ is a double-quadratic well at $T=0$. Hence, in this limit, the phase diagram is that of model 1 of Refs. 14 and 15. At $T>0$ however, this double quadratic well becomes nonconvex in a finite interval of x when $\tau<(2\kappa)^{-1}$ for the Ising model [$\tau<(6\kappa)^{-1}$ for the Heisenberg model]. Thus, it is plausible that the phase diagram at these temperatures be similar to that of model 2 of Refs. 14 and 15. When $\nu=0$ ($J_0=0$), the regions, in the plane (κ,τ) where modulated phases can be found, are easily determined. Indeed, it is sufficient to consider the free energy per atom f_e in the dimerized phase [$x_n=(-1)^n a$]:

$$f_e=\tfrac{1}{2}a^2+4a^2[\kappa-(2\tau)^{-1}]+O(a^4) \quad \text{(Ising)}\ , \tag{4.2a}$$

$$f_e=\tfrac{1}{2}a^2+4a^2[\kappa-(6\tau)^{-1}]+O(a^4) \quad \text{(Heisenberg)}\ . \tag{4.2b}$$

Hence, a solution $a\neq 0$ can exist only if

$$\tau'<\xi\leq 1\ , \tag{4.3}$$

where $\tau'=\tau/4$ for the Ising model ($\tau'=3\tau/4$ for the Heisenberg model) and

$$\xi\equiv(1+8\kappa)^{-1}\ . \tag{4.4}$$

Note that the other terms of the expansion (4.2) are needed to stabilize the system when the inequality (4.3) is not satisfied.

As shown in Refs. 13–15, the symmetry properties of (4.1) are such that the phase $\omega=P/Q$ becomes the $\omega=(Q-P)/Q$ phase when $\nu\to-\nu$ and, therefore, only the part $\nu\geq 0$ of the phase diagram needs to be considered. The parameter space of the phase diagram is of dimension 3. The chosen parameters are ξ, τ', and ν', where ν' is defined by

$$\nu'\equiv\nu/(4\xi)\ . \tag{4.5}$$

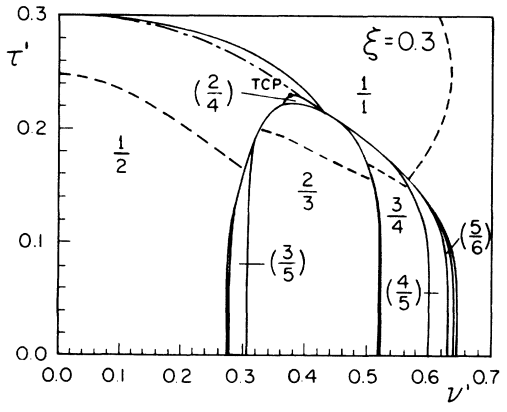

FIG. 1. Phase diagram at $\xi=0.3$ in the (τ',ν') plane. The numbers are values of the winding number ω. The unlabeled regions contain additional commensurate phases. Also shown are separation lines (dashed lines) and magnetic separation lines (dashed-dotted lines) defined in the text. TCP denotes a tricritical point.

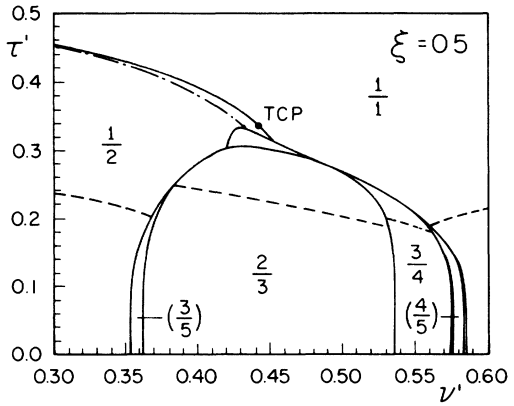

FIG. 2. Same as Fig. 1 for $\xi=0.5$.

The phase diagram at finite temperatures is shown, for the Ising model, as a function of ν' and τ' in Figs. 1–4 for $\xi=0.3$, 0.5, 0.7, and 1.0, respectively. Note that the modulated phases are indeed restricted to the region (4.3).

It is interesting to note from Fig. 4 that only the $\frac{1}{1}$ and $\frac{1}{2}$ nonconvex phases exist when $\xi=1$. Hence, there is no frustration leading to periodically modulated phases when $\kappa=0$. Indeed, in this limit, the effective first-neighbor interaction is repulsive and does not, by itself, favor a particular structure. A nontrivial competition between the external potential and the interactions exist only when both magnetoelastic coupling and first-neighbor elastic interactions are present.

Nonconvex phases exist only for $\tau>0$ (except for the marginal case $\xi=1$) since, at $\tau=0$, $\psi(x)$ is nonconvex only at the isolated unstable point $x=0$. They are located above (to the left of, for the uniform phase of Fig. 1) the *separation lines*[14,15] represented by dashed lines in the figures. As for model 2 of Refs. 14 and 15, some phases (such as the $\frac{3}{5}$ phase) are always convex, and others (as the $\frac{2}{4}$ phase) are always nonconvex though most of the

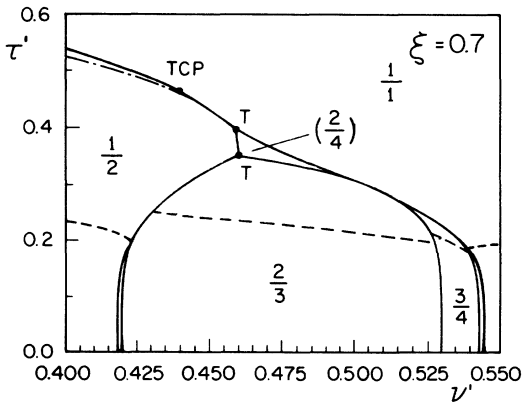

FIG. 3. Same as Fig. 1 for $\xi=0.7$. T denotes a triplet point.

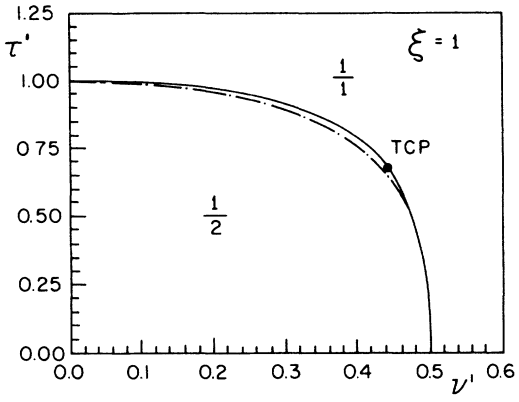

FIG. 4. Same as Fig. 1 for $\xi=1.0$.

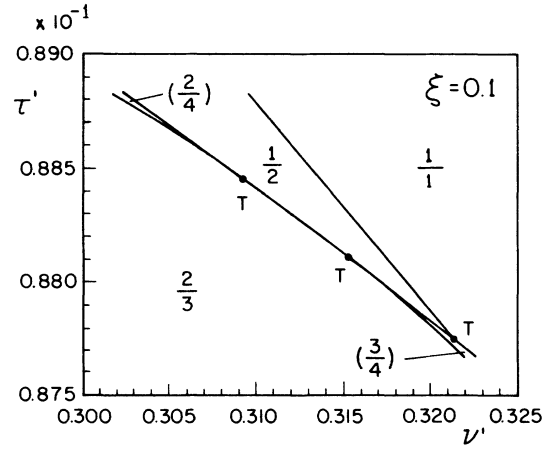

FIG. 6. Phase diagram at the crossing of the $\frac{1}{1}$, $\frac{1}{2}$, $\frac{2}{3}$, $\frac{2}{4}$, and $\frac{3}{4}$ phases for $\xi=0.1$.

phases are both convex and nonconvex in different regions of the phase diagram.

For a given phase of period Q, the fraction ω_J of antiferromagnetic bonds is given by

$$\omega_J=\frac{1}{Q}\sum_{n=1}^{Q}\Theta(x_{n-1}-x_n+\nu)\ . \tag{4.6}$$

The *magnetic separation lines,* represented by dashed-dotted lines in the figures, separate the region where $\omega=P/Q=\omega_J$ from the region $\omega\neq\omega_J=(P+1)/Q$ of the same phase. Almost all of the phases have $\omega_J=\omega$ except the $\frac{1}{2}$ phase where $\omega_J=\frac{2}{2}$ in a narrow region near the uniform phase and the nonconvex P/Q phases, where P and Q have a common divisor such as $\frac{2}{4}$, $\frac{4}{6}$, and $\frac{6}{8}$ where $\omega_J=(P+1)/Q$ everywhere. However, as illustrated in Figs. 5 and 7, there is a region to the left of the magnetic separation line of the $\frac{2}{4}$ phase where $\omega_J=\frac{2}{4}$. This case exists only in the presence of a tricritical point (TCP) (between the $\frac{1}{2}$ and the $\frac{2}{4}$ phases) at which the first-order transition line, to the right of TCP, becomes one of second order, to the left of TCP. In addition, it is interesting to note that this tricritical point collapses in the $\frac{2}{3}$ phase as ξ is increased and has disappeared completely in Figs. 2–4.

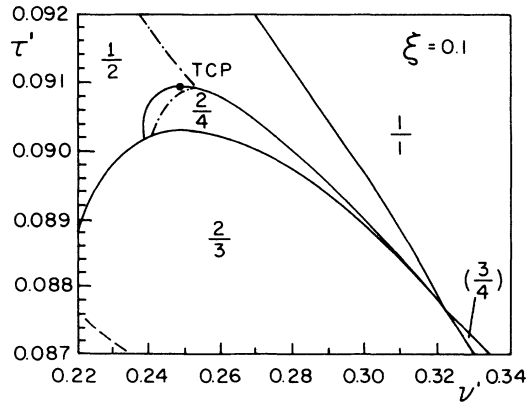

FIG. 5. Phase diagram in the neighborhood of the $\frac{2}{4}$ phase for $\xi=0.1$.

The phase diagram at finite temperature is similar to that of model 2 of Refs. 14 and 15; namely, a devil's-staircase behavior is observed for transitions between convex phases whereas first- and second-order transitions are observed between nonconvex phases. For the same reasons as in Refs. 14 and 15, incommensurate phases should not occur in this model with a finite measure in parameter space.

B. Tricritical point between the uniform and dimerized phases

In contrast with model 2 of Refs. 14 and 15, there is a tricritical point, below which the transition is first order and above which the transition is second order, between the uniform and the dimerized phase for large enough values of ξ (see Figs. 2–4). This point is located precisely by using a Landau-type approach which consists of minimizing the free energy per atoms $f_e(a)$ when $x_n=(-1)^n a$. The dimerization a at equilibrium has to satisfy $\partial f_e/\partial a=0$. For the Ising model, this condition can be written as

$$\cosh(z)-(\zeta z)^{-1}\sinh(z)+\cosh(\Gamma)=0\ , \tag{4.7}$$

where $z\equiv 4a/\tau$, $\Gamma\equiv\nu/(2\tau')$, and $\zeta\equiv\tau'/(2\xi)$. Moreover, we can use the following expansion:

$$\cosh(z)-(\zeta z)^{-1}\sinh(z)$$

$$=\left[1-\frac{1}{\zeta}\right]+\sum_{n=1}^{\infty}\frac{1}{(2n)!}\left[1-\frac{1}{(2n+1)\zeta}\right]z^{2n}\ . \tag{4.8}$$

Hence, dimerization cannot occur for $\zeta>\frac{1}{2}$. A solution $a\neq 0$ grows continuously (second-order transition) from $a=0$ for $\frac{1}{3}<\zeta<\frac{1}{2}$. For $\zeta<\frac{1}{3}$, however, a solution appears discontinuously (first-order transition) at a finite

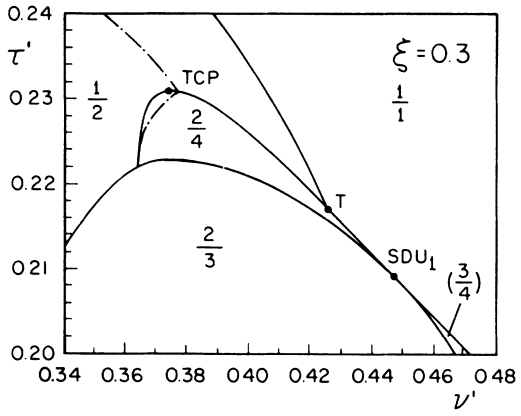

FIG. 7. Same as Fig. 5 for $\xi=0.3$.

value of a. Therefore, the tricritical point is located at $\xi=\xi_T$, $\Gamma=\Gamma_T$, where

$$\xi_T=\tfrac{1}{3}\ , \tag{4.9a}$$

$$\cosh(\Gamma_T)=2\ . \tag{4.9b}$$

This result agrees with the well-known result[11,13,22] for the tricritical point of the Ising incompressible magnetoelastic chain. It is interesting to note that in model (2.1), this tricritical point does not manifest itself in the phase diagram for small values of ξ (see Fig. 1) since, at this point, the ground state of (4.1) is neither the $\frac{1}{1}$ nor the $\frac{1}{2}$ phase.

C. Superdegenerate lines

Figure 5 presents the phase diagram in the neighborhood of the $\frac{2}{4}$ phase for $\xi=0.1$, and Fig. 6 shows more clearly how the $\frac{1}{1}$, $\frac{1}{2}$, $\frac{2}{3}$, $\frac{2}{4}$, and $\frac{3}{4}$ cross each other. As in model 2 of Refs. 14 and 15, the transitions $\frac{2}{4}$-$\frac{1}{2}$, $\frac{1}{2}$-$\frac{2}{3}$, $\frac{1}{2}$-$\frac{3}{4}$, $\frac{3}{4}$-$\frac{2}{3}$, $\frac{3}{4}$-$\frac{1}{1}$, and $\frac{2}{3}$-$\frac{2}{4}$ are all first order and only triple points (identified by T in the figures) exist in this region of the phase diagram. However, it is clear in Fig. 7 that the $\frac{1}{2}$ phase boundary terminates on the $\frac{2}{4}$ phase for $\xi=0.3$. In addition, we have not been able to find a common boundary between the $\frac{1}{1}$ and $\frac{2}{3}$ phases for this value of ξ. A careful examination with the algorithm of Griffiths and Chou reveals that the equilibrium lattice structure in the $\frac{2}{4}$ phase, slightly above the point SDU_1 of Fig. 7, is of the form $(+x_1,-\epsilon,+\epsilon,-x_1)$ over one period where ϵ is small. On the other hand, the equilibrium lattice structure in the $\frac{3}{4}$ phase slightly below the point SDU_1 is of the form $(+x_1,+\epsilon,-\epsilon,-x_1)$. Note that the $\frac{2}{4}$ and the $\frac{3}{4}$ phases are identical when $\epsilon=0$. In this case, we can consider the group of atoms $(-x_1,+x_1)$ as a soliton of the uniform phase. These solitons are noninteracting since they are separated by a sufficiently large number of atoms (two for a Hamiltonian where the range of interaction is limited to first neighbors) at positions corresponding to the uniform phase. Hence, we have infinite degeneracy when $\epsilon=0$ since, starting from this state of period four, we can build an infinite number of other states of the same free energy of separating these solitons by an arbitrary number (≥ 2) of atoms located at $X=0$. If this state is the ground state of F_e at SDU_1, then SDU_1 would be a superdegenerate point[15,18,19] where the ground state of F_e is infinitely degenerate.

To find the superdegenerate points that can exist on the boundary of the $\frac{1}{1}$ phase, we have solved the system of equations (4.6) of Ref. 15 with $K=1$ and $\phi(x)=\psi'(x)$. These equations arise from $\partial F_e/\partial x_n=0$. For a given M ($M=1,2,3,\ldots$), the solution of this system of equations defines a surface in (ξ,τ',ν') space where the phase $(2M+1)/(2m+2)$ has two consecutive atoms at $x=0$. As in Ref. 15, we define the line SDU_M as the line on this surface where the energy is identical to that of the uniform phase. These lines are plotted in the (ξ,ν') plane (see Fig. 8) and in the (ξ,τ') plane (see Fig. 9) for $M=1$, 2, 3, and 4. On these lines, there is an infinite number of states of F_e with the same energy. As explained in Ref. 15, we use the algorithm of Griffiths and Chou to determine which points on these SDU_M lines are superdegenerate points. On the SDU_M lines with $M>1$ and on the portion of the SDU_1 line located to the right of the point Z (see Figs. 8 and 9), the algorithm of Griffiths and Chou

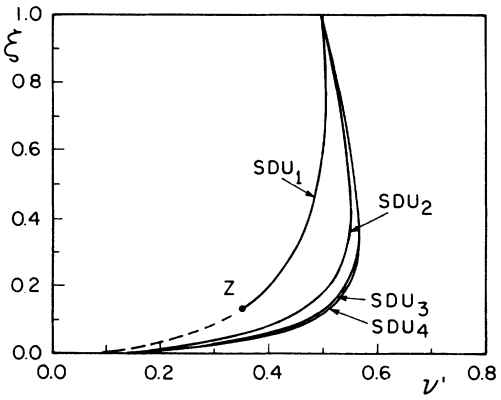

FIG. 8. Superdegenerate lines in the (ξ,ν') plane as defined in the text.

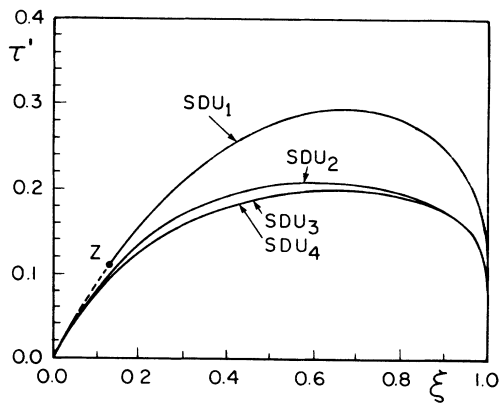

FIG. 9. Same as Fig: 8 in the (ξ,τ') plane.

always gives the $\frac{1}{1}$ phase, indicating that the ground state of F_e on these lines consists of noninteracting solitons with zero creation energy. Hence, these lines are superdegenerate lines. However, the algorithm of Griffiths and Chou gives the $\frac{1}{2}$ phase on the portion of the SDU_1 line located to the left of the point Z (indicated by a dashed line on Figs. 8 and 9); indicating that the ground state of F_e is the $\frac{1}{2}$ phase on this portion of the line.

We can precisely locate the point Z by searching for the point on the SDU_1 line where the $\frac{1}{2}$ phase bifurcates to the $\frac{1}{1}$ phase. Numerically, we obtain the following coordinate for Z:

$$\nu_z' = 0,3\,501\,189\ , \tag{4.10a}$$

$$\xi_z = 0,1\,334\,020\ , \tag{4.10b}$$

$$\tau_z' = 0,1\,129\,648\ , \tag{4.10c}$$

with an uncertainty of one unit in the last digit.

From Figs. 5 and 6, it seems plausible that for $\xi < 0.1$ and $M > 1$, the points SDU_M could be located in the $\frac{1}{2}$ phase. However, a careful numerical examination shows that the phase boundary between the $\frac{1}{1}$ and $\frac{1}{2}$ phases is always located between the points SDU_1 and SDU_2 for $\xi \lesssim 0.01$. Hence the points SDU_M for $M > 1$ are all superdegenerate points.

In addition, the same numerical procedure used in Ref. 15 reveals that the phase diagram near the $\frac{1}{1}$ phase boundary has the same structure as that sketched in Fig. 11 of Ref. 15, namely that each superdegenerate point SDU_M is surrounded only by the nonconvex phases $\frac{1}{1}$, $2M/(2M+1)$, $2M/(2M+2)$, and $(2M+1)/(2M+2)$ which are separated from each other by first-order transitions. Since only a finite number of phases merge to these superdegenerate points, they qualitatively differ from the multiphase point of the ANNNI model.[5]

V. CONCLUSION

By using the numerical algorithm of Griffiths and Chou, we have obtained, in a 3D parameter space, a complex phase diagram for the magnetoelastic model (2.1). At $T=0$, the model is the same as model 1 of Ref. 15 and our numerical results are suggestive of a devil's-staircase behavior. For $T>0$, the phase diagram becomes similar to that of model 2 of Ref. 15; in particular, first- and second-order phase transitions are found among nonconvex phases. In addition, we have found a tricritical point between the uniform and the dimerized phase. Moreover, we have shown that, in contrast with model 2 of Ref. 15, the point SDU_1 can become a superdegenerate point. This result also shows that the situation encountered in the chiral XY model[19] where a superdegenerate point is located between the $\frac{0}{1}$, $\frac{2}{4}$, $\frac{1}{3}$, $\frac{1}{4}$, and $\frac{1}{2}$ phases is a marginal case since this point is located precisely on the $\frac{0}{1}$-$\frac{1}{2}$ transition line. This superdegenerate point is the analog of the point Z of the magnetoelastic model (2.1).

The algorithm of Griffiths and Chou has certainly proven to be useful in obtaining a global and complex phase diagram without postulating, *a priori*, the nature of the phases. Indeed, certain results, such as the existence at finite temperatures of nonconvex phases like $\frac{2}{4}$ and $\frac{4}{6}$ were not easily predictable. However, in order to locate some specific details of the phase diagram, such as superdegenerate points and tricritical points, we had to rely on more precise methods such as the set of equations (4.6) of Ref. 15 and a Landau approach which is based on comparing the free energies of two given phases. These methods, although biased, are powerful when preliminary results, obtained from the algorithm of Griffiths and Chou, justify their use.

ACKNOWLEDGMENTS

We are grateful to Professor R. B. Griffiths and Kevin Hood for useful discussions. This work was supported by the Natural Sciences and Engineering Research Council of Canada and the Fonds pour la Formation de Chercheurs à l'Aide à la Recherche du Québec.

*Present address: Institut für Festkörperforschung der Kernforschungsanlage Jülich GmbH, Postfach 1913, D-5170 Jülich, West Germany.

[1]R. A. Cowley, Adv. Phys. **29**, 1 (1980), and references therein.
[2]A. D. Bruce, Adv. Phys. **29**, 111 (1980), and references therein.
[3]T. De Simone, R. M. Stratt, and J. Tobochnik, Phys. Rev. B **32**, 1549 (1985).
[4]N. Ishimura, J. Phys. Soc. Jpn. **54**, 4752 (1985).
[5]M. E. Fisher and W. Selke, Phys. Rev. Lett. **44**, 1502 (1980).
[6]P. Bak and J. von Boehm, Phys. Rev. B **21**, 5297 (1980).
[7]W. Selke and P. M. Duxbury, Z. Phys. B **57**, 49 (1984).
[8]T. De Simone and R. M. Stratt, Phys. Rev. B **32**, 1537 (1985).
[9]B. Mandelbrot, *Fractals: Form, Chance and Dimension* (Freeman, San Francisco, 1977).
[10]S. Aubry, J. Phys. C **16**, 2497 (1983).
[11]E. Pytte, Phys. Rev. B **10**, 2039 (1974).
[12]M. Marchand, A. Caillé, and R. Pépin, Phys. Rev. B **34**, 4710 (1986).
[13]M. Marchand, Ph.D. thesis, Sherbrooke University, Sherbrooke, Québec, 1987.
[14]M. Marchand, K. Hood, and A. Caillé, Phys. Rev. Lett. **58**, 1660 (1987).
[15]M. Marchand, K. Hood, and A. Caillé, Phys. Rev. B **37**, 1898 (1988).
[16]R. B. Griffiths and W. Chou, Phys. Rev. Lett. **56**, 1929 (1986).
[17]W. Chou and R. B. Griffiths, Phys. Rev. B **34**, 6219 (1986).
[18]The term superdegenerate point is used [see J. L. Lebowitz, M. K. Phani, and D. F. Styer, J. Stat. Phys. **38**, 413 (1985)] to designate a point in parameter space where the ground state is infinitely degenerate. We shall keep this definition for points where the ground state of the free-energy functional (3.1) is infinitely degenerate. Note also that a superdegenerate point need not be a multiphase point (Ref. 5) where an infinite number of phases merge. Indeed, some superdegenerate

points where only a finite number of phases merge have been found, for instance, in Refs. 15 and 19 and in this work.

[19]C. S. O. Yokoi, L. Tang, and W. Chou, Phys. Rev. B **37**, 2173 (1988).

[20]J. W. Bray, L. V. Interrante, I. S. Jacobs, and J. C. Bonner, in *Extended Linear Chains Compounds,* edited by J. S. Miller (Plenum, New York, 1982), Vol. 3, pp. 353–415, and references therein.

[21]M. Steiner, J. Villain, and C. G. Windsor, Adv. Phys. **25**, 87 (1976).

[22]K. A. Penson, A. Holz, and K. H. Bennemann, Phys. Rev. B **13**, 433 (1976).